Pramāṇa Vol. 2, No. 4, 1974, pp 179–188. Printed in India.

Lattice dynamics of beryllium

B A DASANNACHARYA, P K IYENGAR, R V NANDEDKAR, K R RAO, A P ROY and C L THAPER
Nuclear Physics Division, Bhabha Atomic Research Centre, Trombay, Bombay 400085

MS Received 15 January 1974

Abstract. Phonon frequencies in beryllium along the principal symmetry directions have been determined by means of the slow neutron inelastic scattering technique. The data are analysed in terms of a six-neighbour force constant model and the force constants are evaluated. It is concluded that strong tensor forces are present in beryllium and the importance of this finding to basic theories of lattice dynamics is pointed out.

Keywords. Lattice dynamics, phonons, beryllium, neutron scattering.

1. Introduction

This paper presents extensive measurements of phonon dispersion curves in beryllium along ΓA, ΓM, ΓKM, AL and AH directions using neutron spectrometry. The experiments were carried out on a filter-detector spectrometer (FDS) and a triple-axis spectrometer (TAS). Earlier measurements (Schmunk *et al* 1962, Schmunk 1966) were restricted mainly to ΓA and ΓM directions. In section 2 of this paper the experimental details are described and the results are presented in section 3. Some of these results have been reported earlier (Thaper *et al* 1971, Roy *et al* 1973). The analysis and discussion are given in section 4. The data are analysed in terms of a six-neighbour force constant model and the force constants are evaluated. On this basis it is shown that if one wants to arrive at a reasonable theoretical model to describe the lattice dynamics of hexagonal metals it is not sufficient to carry out measurements along ΓA and ΓM alone. From the measurements it is further concluded that strong tensor forces involving many body interactions are present in beryllium. Presence of such forces can be unequivocally proven by an examination of the sequence of frequencies at the point K in the Brillouin zone.

2. Experiment

2·1 *Sample*

The experiments were performed on two different crystals. Crystal #1 was a slab of dimension 6·5 cm × 4·3 cm × 2·2 cm and most of the measurements on this were made on the TAS. Crystal #2 (7·1 cm × 3·8 cm × 1·4 cm) was utilised for most of the measurements on FDS. The quality of crystal #1 was

somewhat better than that of crystal #2 as judged from the measured shapes of some rocking curves. Therefore, some phonons were measured on both the spectrometers on the better crystal (#1), as a check on the accuracy of the measurements. In general, the measurements on the crystals #1 and #2 on the separate spectrometers gave fair agreement (Thaper *et al* 1971).

2.2 *Measurements*

The FDS has not been used earlier in a systematic way to measure phonon frequencies. The reason for this mainly lies in the fact that a filter allows all neutrons above a certain wavelength to pass through, resulting in a poor resolution in the outgoing neutron wavevector k'. Further, unlike in a TAS where the analyser function is a Gaussian centered around the average outgoing wavevector, one has to deal here with an asymmetrical analyser function. Because of these reasons it has been believed rather erroneously that FDS cannot be used for accurate phonon work. It was therefore necessary to first justify that the FDS can indeed be used for such measurements. This was done in our laboratory recently both on experimental as well as theoretical basis and forms the subject of a separate paper (Thaper *et al* 1973). The main conclusions of this paper were the following :

(*a*) It is possible to measure phonon frequencies accurately using a FDS with a beryllium oxide filter, if one assumes the average outgoing energy $E' = 2{\cdot}5$ meV and average outgoing wavevector $| k' | = 1{\cdot}1$ A^{-1}. With these values of E' and k' the FDS can be used just like a TAS, even if the slopes of the phonon branches are fairly large. The intensities of the neutron groups (in the available regions of reciprocal space) measured using FDS are larger than in the conventional TAS.

(*b*) Utilising the resolution formulae given earlier it is possible to predict the shapes of neutron groups theoretically with reasonable accuracy, and

(*c*) The FDS shows focusing properties similar to those of the TAS. It may be remarked here that a somewhat different method has been used by other workers (Haywood and Collins 1971, Bergsma 1970) to measure flat phonon branches.

The filter in the present measurements consisted of a combination of a block of beryllium oxide of size 10 cm × 5 cm × 5 cm preceded by beryllium made up of 6 slabs of size 10 cm × 0·6 cm × 5 cm each. The beryllium slabs faced the sample and were interleaved with cadmium to minimize the contribution of Bragg and multiply scattered neutrons. The spectrometer was mainly operated in the "constant-Q" and "constant-E" modes. With the energy and wavevector resolutions of the present experiments both the "constant-Q" "constant-E" modes of operation were unsatisfactory for some points. The phonons on Δ_1 and Δ_2 branches along ΓA for q/q_m between 0·9 and 1·0 were measured with the spectrometer programmed to scan along the normal to the dispersion curve. Table 1 lists the scattering planes and reciprocal lattice points (figure 1) around which data were collected for various phonon branches. Inelastic structure factors calculated by Schmunk *et al* (1962) were used as the guidelines for selecting the points for measurements along ΓA and ΓM. The structure factors for ΓKM were computed using the modified axially symmetric force constants given by DeWames *et al* (1965) and these are shown in figure 2 *a*.

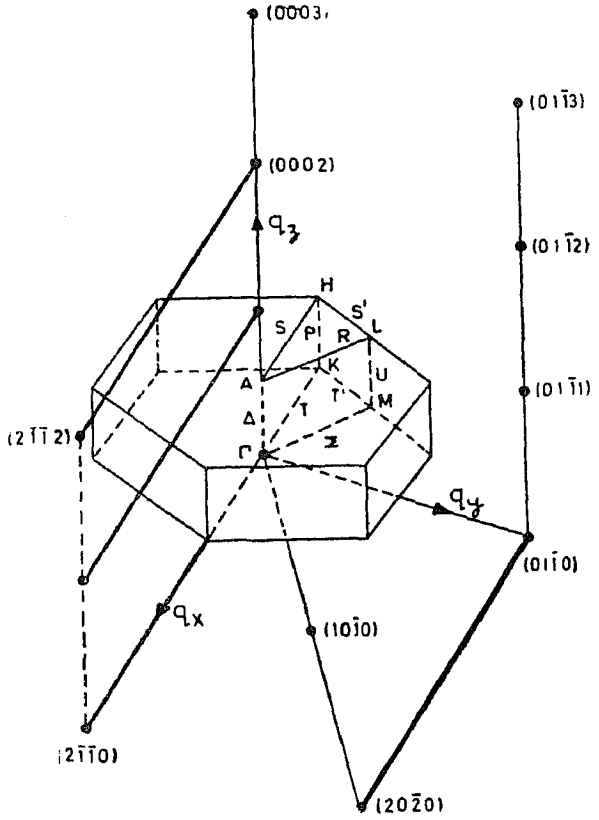

Figure 1. Top half of the first Brillouin zone for a hexagonal lattice. The reciprocal lattice points around which measurements were made are also shown.

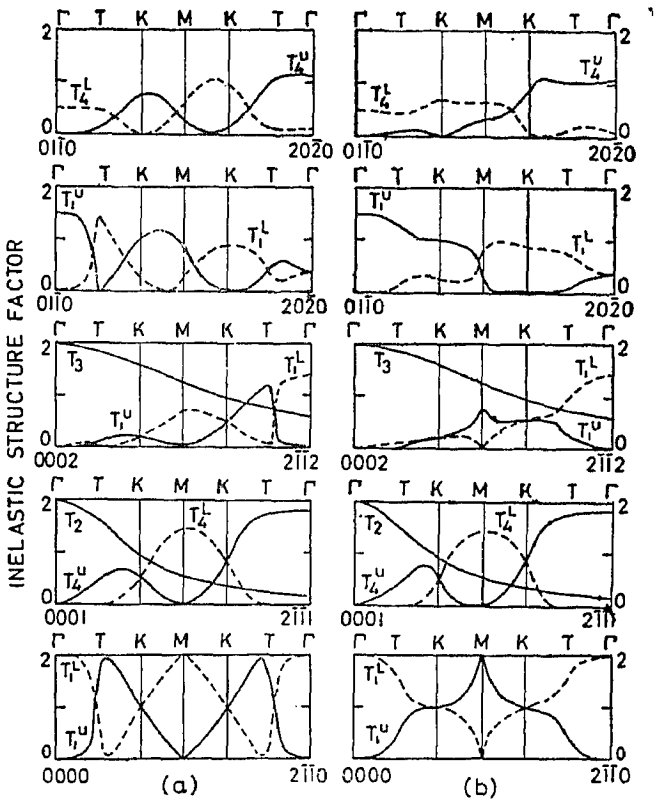

Figure 2. Inelastic structure factor calculations for the ΓKM branches along various lines (shown as thick lines in figure 1) in the reciprocal space using (*a*) the MAS model force constants given by DeWames *et al* (1965) and (*b*) the force constant model discussed in the text.

Some typical neutron groups and their calculated shapes are shown in figure 3 as illustrations. Details of focusing observed on the FDS can be found in the paper by Thaper *et al* (1973).

The measurements on the TAS were carried out in the "constant-E" mode of operation with fixed incoming energy E_0, which was chosen to be 0·09 eV except for some low energy transfer experiments where E_0 was changed to 0·04 eV. The spectrometer was operated in the energy loss mode for the higher incident energy and in energy gain mode for the lower one. The reciprocal lattice points around which the measurements were made are included in table 1. Measurements of phonons with frequencies higher than 12 THz posed intensity problems. Therefore, such frequencies were measured using the FDS. Measurements along ΓKM, AL and AH were performed entirely on the FDS.

3. Results

The results of our measurements are given in figures 4–6 and the frequencies are tabulated in table 2. The labelling of the branches is given in accordance with standard group-theoretical notations (Warren 1968). The zone centre frequencies of 13·8 THz (459 cm^{-1}) and 20·1 THz (669 cm^{-1}) have been observed for the first time. The former frequency agrees very well with the one reported in recent Raman

Table 1. Choice of reciprocal lattice points for measuring various phonon branches

Scattering plane	Branch index	Reciprocal lattice point	Scattering plane	Branch index	Reciprocal lattice point
$(q_y - q_z)$	Δ_1	(0002), $(01\bar{1}2)$, (0004)*	$(q_x - q_y)$	Σ_4^U	$(2\bar{1}\bar{1}0)$
	Δ_2	$(01\bar{1}3)$		Σ_4^L	$(10\bar{1}0)$, $(2\bar{1}\bar{1}0)$*
	Δ_5	$(01\bar{1}1)$		T_1^L	$(20\bar{2}0)$
	Δ_6	$(01\bar{1}2)$, $(02\bar{2}1)$*		T_4^U	$(20\bar{2}0)$
				T_4^L	$(20\bar{2}0)$
	Σ_1^U	$(01\bar{1}2)$			
	Σ_1^L	$(01\bar{1}2)$, $(02\bar{2}1)$*, $(01\bar{1}0)$*	$(q_x - q_z)$	T_1^U	$(2\bar{1}\bar{1}2)$
	Σ_3^U	(0003)		T_1^L	$(2\bar{1}\bar{1}0)$
	Σ_3^L	$(01\bar{1}1)$, $(0\bar{1}13)$*		T_3	$(2\bar{1}\bar{1}1)$, $(2\bar{1}\bar{1}0)$, (0003)
				T_3	$(2\bar{1}\bar{1}2)$

* Measurements made in a triple-axis spectrometer. The rest refer to the filter-detector spectrometer.

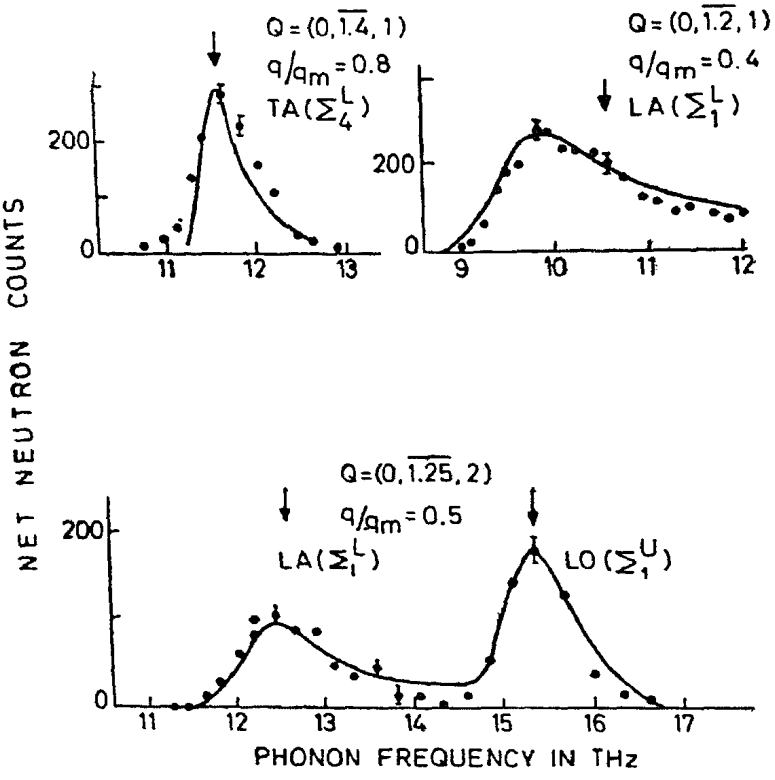

Figure 3. Some typical examples of phonons observed in beryllium using the filter-detector spectrometer. Solid lines are the calculated shapes of neutron groups.

scattering measurements (455 cm^{-1}) (Feldman *et al* 1968). The dispersion curves show a general qualitative agreement with the measurements of Schmunk (1966); the present data however, show less scatter. A quantitative comparison between the two shows differences along the Δ_1, Δ_5 and Σ_1^U branches.

4. Analysis

4.1 *Force constant models*

It is not uncommon to analyse the measured phonon dispersion curves in hcp metals in terms of modified axially symmetric (MAS) model by fitting the calculations

Table 2. Phonon frequencies+ of Be at 297 K in THz. Notations as in figure 1.

q_x	T_1^U, $T_1'^U$
0·20	14·45
0·30	16·00
0·35	16·90
0·40	17·65
0·48	17·95
0·53	18·05
0·60	18·60
0·80	18·10
0·90	17·75

q_x	T_1^L, $T_1'^L$
0·20	10·50
0·25	11·75
0·30	12·55
0·40	13·70
0·45	14·10
0·50	14·20
0·53	14·15
0·75	14·70
0·80	15·05
0·90	16·00

q_x	T_2, T_2'
0·20	19·20
0·33	18·35
0·40	17·55
0·47	16·70
0·53	15·90
0·60	15·35

q_x	T_3, T_3'
0·53	13·00
0·60	13·90
0·67	15·00
0·80	16·60

q_x	T_4^U, $T_4'^U$
0·10	13·80
0·20	14·60
0·30	15·50
0·40	16·20
0·45	16·70
0·50	17·05
0·60	16·35
0·67	15·80
0·75	16·30

q_x	T_4^L, $T_4'^L$
0·42	11·00
0·50	12·25
0·60	13·20
0·67	14·00
0·75	13·35
0·80	12·50
0·90	11·85
1·00	11·75

q_Y	Σ_1^U
0·10	13·87
0·20	14·25
0·40	15·05
0·50	15·40
0·60	15·82
0·70	16·25
0·80	16·47
0·90	16·75
1·00	16·82

q_Y	Σ_1^L
0·09	3·00*
0·12	4·00*
0·20	6·00*
0·24	7·00*
0·28	8·00*
0·32	9·00*
0·36	10·00*
0·42	11·00*
0·48	12·00*
0·50	12·55
0·53	13·00*
0·60	13·82
0·62	14·00*
0·70	15·03
0·74	15·40
0·81	16·00

q_Y	Σ_3^U
0·10	19·92
0·20	19·80
0·30	19·52
0·40	19·17
0·50	18·55
0·60	18·25
0·70	17·65
0·80	17·32
0·90	17·07
1·00	17·00

q_Y	Σ_3^L
0·38	7·00*
0·40	7·75
0·43	8·00*
0·50	8·50*
0·50	8·78
0·55	9·00*
0·62	10·25
0·65	10·00*
0·70	10·82
0·75	11·00*
0·80	11·70
0·85	12·00*
0·90	12·30
1·00	12·60

q_Y	Σ_4^U
0·00	13·85
0·20	13·90
0·40	14·75
0·50	15·07
0·60	15·30
0·80	16·00
1·00	16·60

q_Y	Σ_4^L
0·18	4·00*
0·26	5·00*
0·27	6·00*
0·34	7·00*
0·52	9·07
0·60	9·65
0·70	11·00
0·80	11·30
0·90	11·78
1·00	11·75

q_z	Δ_6
0·36	5·00*
0·42	5·70*
0·54	7·00*
0·63	7·70*
0·70	8·85
0·80	9·65
0·87	10·15

q_z	Δ_1
0·31	6·05
0·36	7·00*
0·41	8·05
0·48	8·80*
0·51	9·15
0·52	9·00*
0·56	9·87*
0·58	10·15
0·61	10·15
0·63	11·00*
0·64	10·75*
0·72	11·30
0·74	11·80*
0·75	12·00*
0·82	12·05
0·82	12·70*
0·84	13·00*
0·86	13·10
0·90	13·80
0·96	14·15

q_z	Δ_2
0·00	20·10
0·10	20·10
0·20	19·87
0·30	19·80
0·40	18·85
0·50	18·45
0·60	17·85
0·70	17·25
0·80	16·70
0·83	16·65
0·90	16·00
0·96	15·35
0·98	15·25
1·00	15·00

q_z	Δ_5
0·00	13·75
0·10	13·75
0·20	13·62
0·30	13·55
0·40	13·33
0·50	13·12
0·60	12·65
0·70	12·25
0·80	11·90
0·90	11·45
1·00	10·75

q_x, q_Y and q_z are expressed in units of $(2\pi/a)$, $(2\pi/\sqrt{3}a)$ and (π/c) respectively.

+ Based on counting statistics and the shapes of neutrons groups, the errors on the frequencies vary from 1–3%.

* Measurements made in a triple-axis spectrometer. The rest of the measurements were carried out using the filter-detector spectrometer.

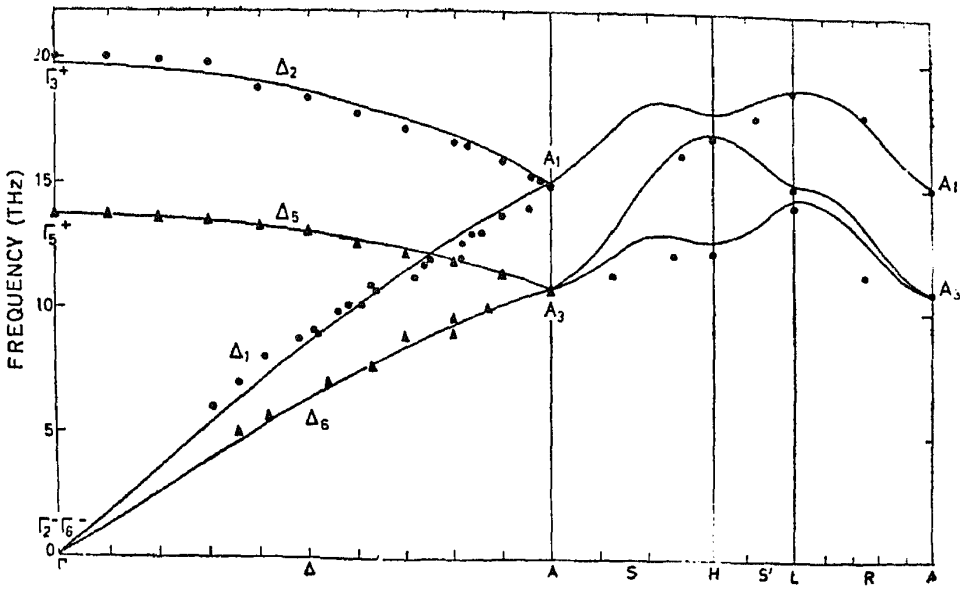

Figure 6. Phonon frequencies along ΓA and on the surface of the Brillouin zone along AH and AL. The solid lines have the same meaning as in figure 4.

particular, it was found that within the framework of MAS model it was impossible to reproduce the observed sequence of T_1 and T_4 branches at the point K (see figures 4 and 7). Irrespective of the number of neighbours taken into consideration one always obtains a doubly degenerate branch between two non-degenerate ones. The reason for this can be readily seen by writing the general expression for the frequencies at K:

$$\nu_{K_5}^2 = \frac{1}{4\pi^2 M}[D_{xx}(q, 11) + \mathrm{Im}D_{xy}(q, 11)] \quad \text{Doubly Degenerate}$$

$$\nu_{K_1}^2 = \frac{1}{4\pi^2 M}[D_{xx}(q, 11) + 2\mathrm{Re}D_{xx}(q, 12) - \mathrm{Im}D_{xy}(q, 11)] \qquad (4.1)$$

$$\nu_{K_3}^2 = \frac{1}{4\pi^2 M}[D_{xx}(q, 11) - 2\mathrm{Re}D_{xx}(q, 12) - \mathrm{Im}D_{xy}(q, 11)].$$

In the MAS model $\mathrm{Im}D_{xy}$ $(q, 11)$ is identically zero and one therefore gets $|\nu_{K_1}^2 - \nu_{K_5}^2| = |\nu_{K_3}^2 - \nu_{K_5}^2|$. In other words the doubly degenerate branch lies exactly in the middle of two non-degenerate ones. In tensor force models, since $\mathrm{Im}D_{xy}(q, 11) \neq 0$ different ordering is possible. For example, one may also have ν_{K_1} and $\nu_{K_3} > \nu_{K_5}$ or ν_{K_1} and $\nu_{K_3} > \nu_{K_5}$. In Be one finds that $\nu_{K_1} > \nu_{K_3} > \nu_{K_5}$ which shows that the MAS model is inherently inadequate for describing the dynamics. As an alternative of the MAS model, mention may be made of the work of Srinivasan and Ramji Rao (1971) who have explicitly taken into account three-body forces following Keating's approach, in addition to two-body forces. But D_{xy} $(q, 11)$ is still real in this model.

To make the model consistent with the present observations tensor force interaction for the nearest neighbours in the basal plane was included. Based on such a model (hereafter called the TF model) with just one more parameter than the earlier MAS model, a new set of force constants was obtained by a non-linear least square fit to the data along ΓA, ΓM and ΓK and the elastic constants. Again

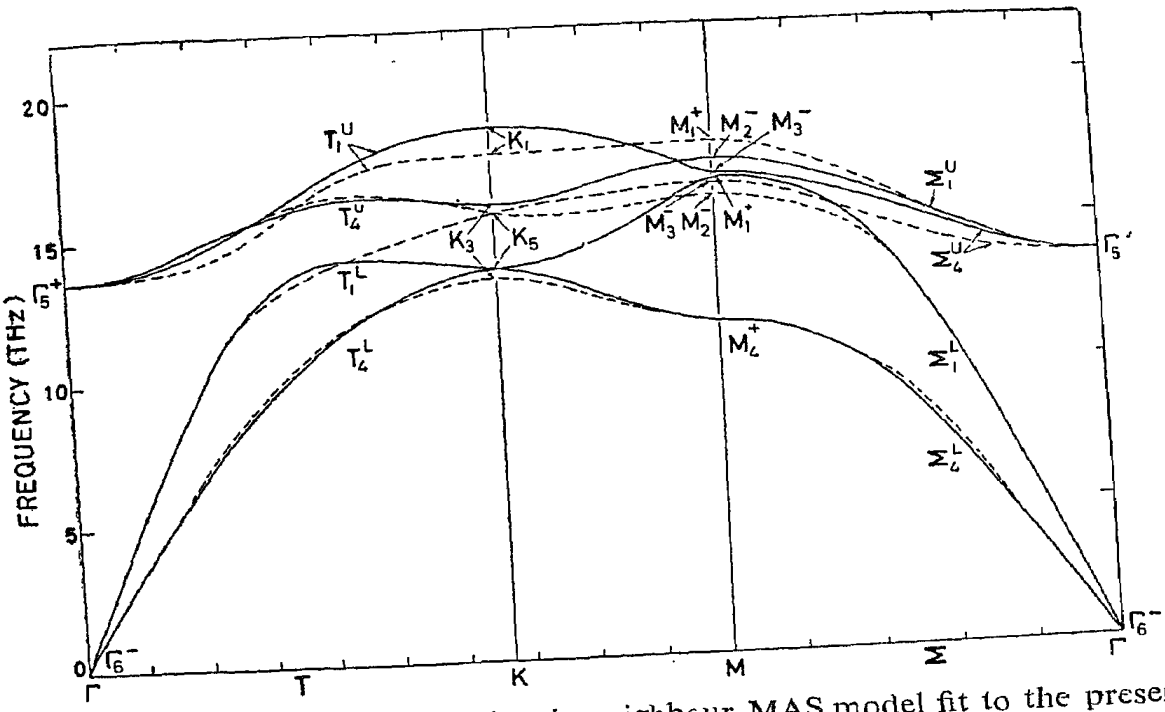

Figure 7. The dashed lines show the six-neighbour MAS model fit to the present data. The solid lines have the same meaning as in figure 4. Note in particular the difference in ordering of the branches in the two models at K and interchange of labelling at M. (– – – – MAS ; ———— TF)

no convergence problem was encountered. The fitted force constants and the calculated elastic constants are given in table 3 and the dispersion curves along the various directions are shown in figures 4 to 6, with continuous lines, as also in figure 7 for comparison with the MAS model results.

Since the MAS model is not adequate for describing the lattice dynamics, especially along ΓK, it was thought that it may be worthwhile examining the inelastic structure factor based on the TF model. This was done for some of the branches along ΓK and is given in figure 2b. These have to be compared with the structure factors calculated using the MAS model and shown in figure 2a. Along the line $(0000) \rightarrow (2\bar{1}\bar{1}0)$ the MAS model predicts an abrupt change in the structure factor which arises from a sudden interchange of polarisation vectors between T_1^U and T_1^L branches at $q = 0{\cdot}33\ (2\pi/a)$. This change-over is absent in the TF model. There is also a change-over in the structure factors at the point M along the same line; this, however, is merely a consequence of interchange of labelling of the branches (see figure 7 for labelling). Measurements of the intensities of these phonons would provide further evidence for the validity of the TF model. However, since the phonon frequency measurements along ΓK were carried out on the FDS, which has a restricted coverage in the reciprocal space, a systematic investigation of the intensity of neutron groups around regions of interest was not feasible.

4.2 *Basic Calculations*

Several microscopic calculations of the dispersion curves of hcp metals have been carried out based on the pseudopotential theory (King and Cutler 1970, and the references cited therein). King and Cutler (1970) obtain good agreement with experimental results along ΓA and ΓM in beryllium, using what the authors call a non-local pseudopotential approach. But in all these calculations which employ second order perturbation theory in the pseudopotential starting with plane waves the electronic contribution to the dynamical matrix $D_{xy}^{E}(q, 11)$ can be expressed as

Table 3a. Best fit six-neighbour force model for beryllium.

Neighbour	Force constant	dyne/cm.	Neighbour	Force constant	dyne/cm.
1	δ_1	2132	4	β_{4x}	3605
	ϵ_{1x}	3678		$a_4 + \beta_{4z}$	5358
	ϵ_{1z}	1878			
2	a_2	13285	5	δ_5	53
	β_{2x}	3265		ϵ_{5x}	230
	β_{2z}	1105		ϵ_{5z}	1306
	δ*	−6223			
3	δ_3	220	6	a_6	1639
	ϵ_{3x}	−2534		β_{6x}	688
	ϵ_{3z}	−3416		β_{6z}	1292

* For the definition of the tensor force constant δ *see* Iyengar *et al* (1965). The remaining MAS model force constants are defined following DeWames *et al* (1965).

Table 3b. Comparison of calculated and experimental elastic constants for beryllium (in units of 10^{11} dyne/cm^2).

Elastic Constant	Experimental[a]	Calculated	Elastic Constant	Experimental	Calculated
C_{11}	29·23	27·62	C_{66}	13·28	11·85
C_{33}	33·64	31·31	C_{13}	1·40	1·29
C_{44}	16·25	15·83[b] 16·53[c]			

a Smith and Arbogast (1960).

b Calculated from the expression of C_{44} as obtained by taking the limiting slope ($q \to 0$) along ΓM.

c From the limiting slope along ΓA. It may be noted that the condition of rotational invariance leads to the identity of above two expressions for C_{44}.

$$D_{xy}^{E}(q, 11) = \text{const.} \sum_{\tau} [(\tau+q)_x (\tau+q)_y E(|\tau+q|) - (\tau)_x (\tau)_y (1+\cos \tau \cdot r_{12}) E(|\tau|)] \quad (4.2)$$

where r_{12} is the separation of the atoms 1 and 2 in the unit cell, τ is a reciprocal, lattice vector and $E(|Q|)$ is Harrison's energy-wavenumber characteristics which is real. Therefore $D_{xy}^{E}(q, 11)$ is real and the same is true for $D_{xy}^{c}(q, 11)$, arising from the direct coulomb interaction between the ions. Thus, $\mathrm{Im}D_{xy}(q, 11)$ is zero as in the MAS model. It may be stated in general that any calculation which involves pairwise interactions between the particles, irrespective of whether it is based on a force constant model or pseudopotential theory, predicts a degenerate frequency $\nu = (D_{xx}(q, 11)/4\pi^2 M)^{\frac{1}{2}}$ (see equation 4.1) at K, with one non-degenerate frequency higher and another lower, contrary to the observation in some hcp substances.

Bertoni *et al* (1973) have recently reported a first principle calculation of the lattice dynamics of beryllium where the total electron energy up to the third order in the electron-ion pseudopotential has been considered and its explicit contribution to the dynamical matrix has been evaluated. The authors find that this scheme, which in effect gives rise to three body forces, leads to the correct sequence of the branches at K apart from improving the overall agreement with experiments.

5. Summary

Detailed measurements of phonon dispersion curves in Be along ΓA, ΓM, ΓKM, AL and AH are reported. Force constants based on a six neighbour model, described in the text, are evaluated. It is shown that in hcp metals it is necessary to make measurements along directions other than ΓA and ΓM in order to evaluate realistic force constants. The sequence of branches at the point K is shown to throw light on the nature of forces in hcp substances. In particular, in beryllium they prove the existence of strong tensor forces. Ordering similar to that in beryllium is found in many other hcp metals (Roy *et al* 1973). The importance of this finding in relation to basic theories of lattice dynamics is pointed out.

Acknowledgements

We thank V C Sahni, S K Sinha and G Venkataraman for valuable discussions, V Bortolani for sending the results of his calculation prior to publication and P R Vijayaraghavan for non-linear least square fitting programme. We gratefully acknowledge the technical assistance given by T Srinivasan.

References

Bergsma J 1970 RCN-121, Petten, The Netherlands
Bertoni C M, Bortolani V, Calandra C and Nizzoli F 1973 (Preprint)
DeWames R E, Wolfram T and Lehman G W 1965 *Phys. Rev.* A **138** 717
Feldman D W, Parker Jr J H and Ashkin M 1968 *Phys. Rev. Lett.* **21** 607
Haywood B C and Collins M F 1971 *J. Phys.* C **4** 1299
Iyengar P K, Venkataraman G, Vijayaraghavan P R and Roy A P 1965 *J. Phys. Chem. Solids, Suppl.* **1** 223
King W F and Culter P H 1970 *Phys. Rev.* **B2** 1733
Roy A P, Dasannacharya B A, Thaper C L and Iyengar P K 1973 *Phys. Rev. Lett.* **30** 908
Schmunk R E 1966 *Phys. Rev.* **149** 450
Schmunk R E, Brugger R M, Randolph P D and Strong K A 1962 *Phys. Rev.* **128** 562
Sinha S K, Brun T O, Muhlestein L D and Sakurai J 1970 *Phys. Rev.* **B 1** 2430
Smith J F and Arbogast C L 1960 *J. Appl. Phys.* **31** 99
Srinivasan R and Ramji Rao R 1971 *J. Phys. Chem. Solids* **32** 1769
Thaper C L, Rao K R, Dasannacharya B A, Roy A P and Iyengar P K 1971 *Phonons* ed M A Nusimovici (Flammarion, Paris) p 140
Thaper C L, Dasannacharya B A and Iyengar P K 1973 *Nucl. Instrum. Methods* **113** 15
Upadhyaya J C and Verma M P 1973 *J. Phys. F* **3** 640
Wakabayashi N, Sinha S K and Spedding F H 1971 *Phys. Rev.* **B 4** 2398
Warren J L 1968 *Rev. Mod. Phys.* **40** 38